Impact of valence fluctuations on the electronic properties of $RO_{1-x}F_xBiS_2$ (R = Ce and Pr)

S. Dash,[1] T. Morita,[1] K. Kurokawa,[1] Y. Matsuzawa,[1] N. L. Saini,[2] N. Yamamoto,[3] Joe Kajitani,[3] R. Higashinaka,[3] T. D. Matsuda,[3] Y. Aoki,[3] and T. Mizokawa[1]

[1]*Department of Applied Physics, Waseda University, Tokyo 169-8555, Japan*

[2]*Dipartimento di Fisica, Universitá di Roma "La Sapienza" - Piazzale Aldo Moro 2, 00185 Roma, Italy*

[3]*Department of Physics, Tokyo Metropolitan University, Hachioji 192-0397, Japan*

(Received 18 May 2018; revised manuscript received 20 August 2018; published 1 October 2018)

We have investigated the electronic properties of BiS_2-based superconductors by using x-ray photoemission spectroscopy (XPS). In going from $x = 0.3$ to 0.5 in $PrO_{1-x}F_xBiS_2$, the Pr $3d$ and Pr $4d$ peaks are shifted by $\sim 0.10 \pm 0.05$ eV from the Fermi level, partially consistent with the electron doping. In $PrO_{1-x}F_xBiS_2$, the Pr^{3+}-Pr^{4+} mixed valence remains unchanged with the electron doping from $x = 0.3$ to 0.5. In $CeO_{1-x}F_xBiS_2$, the doped electrons for $x = 0.5$ almost suppress the Ce^{3+}-Ce^{4+} valence fluctuation. Although the core-level peaks are also shifted by $\sim 0.10 \pm 0.05$ eV towards the higher-binding-energy side with the electron doping from $x = 0$ to 0.5 in $CeO_{1-x}F_xBiS_2$, the Bi $4f_{7/2}$ binding-energy shift is higher in the Pr system compared with the Ce system. The present results suggest that the doped electrons increase orbital occupations in the rare-earth $4f$ orbitals at the valence band and show valence fluctuations differently in the two systems.

DOI: 10.1103/PhysRevB.98.144501

I. INTRODUCTION

After the discovery of BiS_2-based superconductors in $Bi_4O_4S_3$ by Mizuguchi *et al.* [1] in 2012, extensive studies [2–4] including R(O, F)BiS_2 systems (R = rare-earth element) [5–19] have been done. R(O, F)BiS_2 contain alternatively stacked $RO_{1-x}F_x$ block layers and BiS_2 layers, and conductivity is enhanced by increasing x in the block layer, which introduces electrons to the electronically active BiS_2 layer to exhibit the superconductivity at low temperature [20]. The electronic properties of R(O, F)BiS_2 are governed by the Fermi surfaces constructed from the Bi $6p_x$ and $6p_y$ orbitals, whereas the magnetic properties are related to the RE $4f$ orbital occupation [21–23]. In addition, strong electron-phonon coupling has been reported in $Bi_4O_4S_3$ [3] and $LaO_{0.5}F_{0.5}BiS_2$ [24–27]. On the other hand, spin and orbital fluctuation due to electron-electron interaction are seen with the Fermi-surface nesting in $LaO_{0.5}F_{0.5}BiS_2$ [21]. Because a quasi-one-dimensional Bi $6p_x/p_y$ character is involved with the Fermi-surface nesting [21,28], it would be quite interesting to investigate and understand the role of doped electrons in $RO_{1-x}F_xBiS_2$ superconductors [29].

In $CeO_{1-x}F_xBiS_2$, for $x \leqslant 0.4$, the system is in the Ce^{3+}-Ce^{4+} valence fluctuation regime, while for $x > 0.4$ the system is in the Kondo regime where valence fluctuation is suppressed such that superconductivity and the long-range ferromagnetic orderings (Ce-S-Ce superexchange) appear at low temperature [30]. This shows that the electron doping is crucial in controlling the superconductivity and the magnetism in BiS_2-based superconductors [31]. Angle-resolved photoemission spectroscopy (ARPES) shows that the area of the Fermi surfaces in $CeO_{1-x}F_xBiS_2$ is inconsistent with the nominal F [22,32,33]. This discrepancy between the doping level and the Fermi-surface area suggests that some electrons are localized instead of contributing to the Fermi surfaces. Recently, a resonant ARPES study by Sugimoto *et al.* has shown that the added electrons to the Fermi surface rather increase the occupations to the localized Ce $4f$ orbital hybridized with the Bi $6p_z$ [34]. This genuinely requires further support from the core-level spectroscopy to elucidate the orbital occupations and valence state involved with electron doping in $CeO_{1-x}F_xBiS_2$.

Compared with $CeO_{1-x}F_xBiS_2$, the electronic properties of $PrO_{1-x}F_xBiS_2$ are less studied. The system is semiconducting for $x = 0$, and superconductivity appears for $x =$ 0.1 to 0.7 at low temperature [15]. T_c increases from 2.4 to 4.1 K upon electron doping from $x = 0.3$ to 0.5 in $PrO_{1-x}F_xBiS_2$ [18]. The lattice parameter along the c axis decreases upon electron doping, as above. Although the presence of Pr^{3+}-Pr^{4+} valence fluctuation was examined in $PrO_{1-x}F_xBiS_2$ ($x = 0.13, 0.23$) by using x-ray photoemission spectroscopy (XPS) by Ishii *et al.* [35], the XPS results were not analyzed quantitatively and the doping effects on the valence fluctuation were not clarified. In this paper, we have studied the core-level photoemission spectra to elucidate the F doping effect and the Ce or Pr valence fluctuation in $CeO_{1-x}F_xBiS_2$ ($x = 0, 0.5$) and $PrO_{1-x}F_xBiS_2$ ($x = 0.3, 0.5$) in a quantitative way.

II. METHOD

High-quality single crystals of $PrO_{1-x}F_xBiS_2$ ($x = 0.3$, 0.5) and $CeO_{1-x}F_xBiS_2$ ($x = 0$, 0.5) were prepared by using the CsCl flux method as described elsewhere [17–19]. The F doping level is given by the nominal value [17]. Photoemission spectroscopy at room temperature was carried out with a JEOL JPS9200 analyzer using a Mg Kα (1253.6 eV) source. The total energy resolution was about 1.0 eV. The base pressure of the measuring chamber was 2×10^{-6} Pa. Each

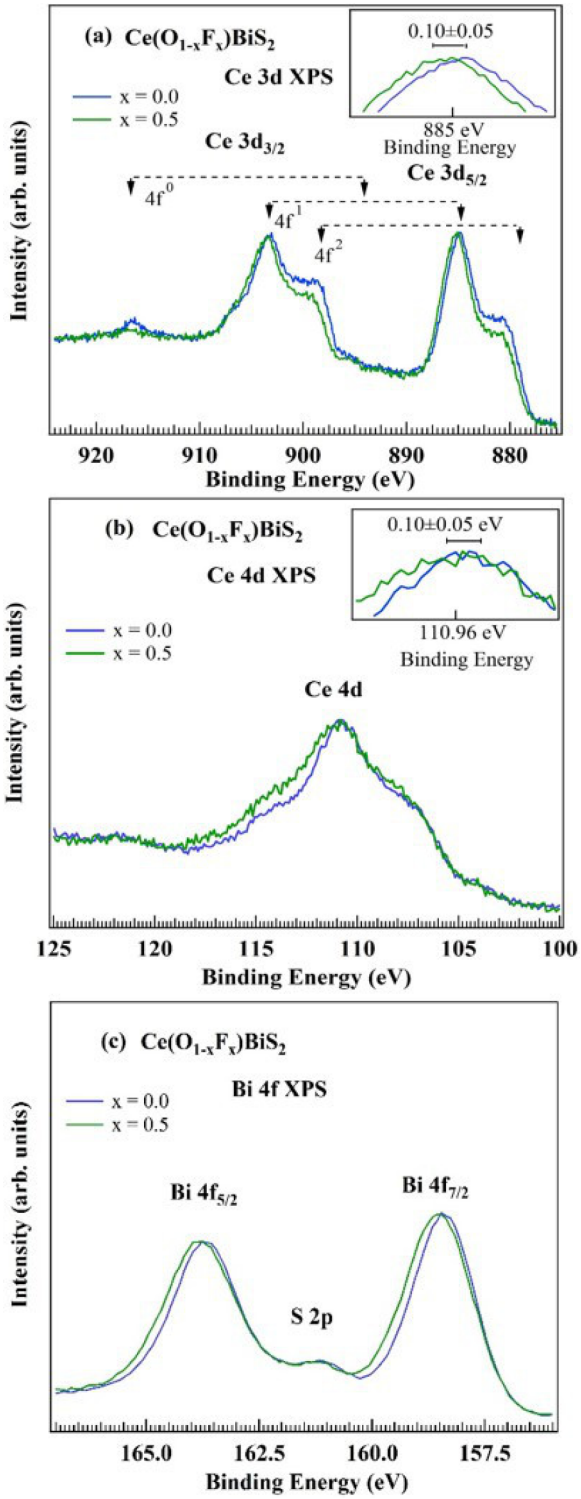

FIG. 1. XPS of (a) Ce $3d$, (b) Ce $4d$, and (c) Bi $4f$ from $CeO_{1-x}F_xBiS_2$ ($x = 0, 0.5$) at room temperature.

spectrum is normalized by its peak intensity and the binding energy is calibrated by using Au $4f$ at 84.0 eV.

III. RESULTS AND DISCUSSION

In Fig. 1(a), the Ce $3d$ peaks of $CeO_{1-x}F_xBiS_2$ ($x = 0$, 0.5) shift by $\sim 0.10 \pm 0.05$ eV toward higher binding energy

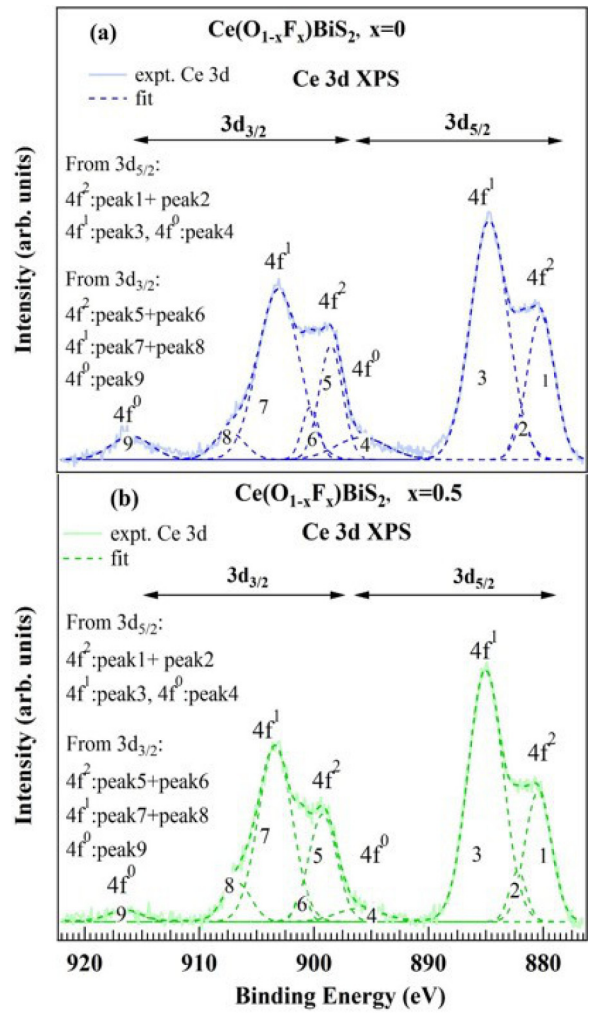

FIG. 2. XPS of Ce $3d$ with Gaussian fittings from $CeO_{1-x}F_xBiS_2$ for (a) $x = 0$ and (b) $x = 0.5$ at room temperature.

from $x = 0$ to 0.5, as shown in the inset. The direction of the Ce $3d$ shifting is consistent with electron doping. The Ce $3d$ XPS spectra show the presence of main peaks $4f^1$, satellite peaks $4f^2$ for Ce^{3+}, and satellite peaks $4f^0$ for Ce^{4+} valence [36,37]. It can be seen that the $4f^0$ (Ce^{4+}) contribution from the $3d_{3/2}$ component decreases with respect to $4f^1$ with doping, consistent with the earlier XAS study [30]. The detailed analysis of the Ce $3d$ peak of $CeO_{1-x}F_xBiS_2$ ($x = 0$, 0.5) is explained later in Fig. 2. Because the resonant-photoemission study earlier revealed that F doping tunes the number of electrons mixed with localized Ce $4f$ in the Kondo regime instead of contributing to the Fermi surface [34], a significant spectral weight transfer within the $4f^0$, $4f^1$, and $4f^2$ peaks of Ce $3d$ [Fig. 1(a)] with electron doping can be seen. The initial states are given by $\alpha 4f^0 + \beta 4f^1 + \gamma 4f^2$ due to mixed valence ($\alpha^2 + \beta^2 + \gamma^2 = 1$). The final states are given by $\alpha' c4f^0 + \beta' c4f^1 + \gamma' c4f^2$, ($\alpha'^2 + \beta'^2 + \gamma'^2 = 1$) and c represents a core hole at the $3d$ level or at the $4d$ level [36]. The $4f^0$, $4f^1$, and $4f^2$ are different states with the U_{ff} (Coulomb repulsion between $4f$ electrons) and the U_{fc} (core hole interaction with $4f$ electrons). In Ce $4d$, apart from shifting towards the high-binding-energy side [see

inset of Fig. 1(b)], the shoulder peaks around the main peak $4f^1$ (~111 eV) in Fig. 1(b) vary with doping, indicating the importance of intra-atomic multiplet coupling and solid-state hybridization [38]. In Fig. 1(c), the Bi $4f$ peaks show a shift of $\sim 0.10 \pm 0.01$ eV toward high binding energy due to electron doping from $x = 0$ to 0.5 in $CeO_{1-x}F_xBiS_2$. The valence decrease of Ce with x should reduce the Ce $3d$ and $4d$ binding energy. On the other hand, by adding electrons at the valence band, all the core-level peaks move away from the Fermi level with x, as seen in Fig. 1. In the present case, the doping effect is dominant compared with the valence effect since the shift of Ce $3d$ is similar to that of Bi $4f$.

It was earlier reported that superconducting and ferromagnetic phase evolves with a different local environment in $CeO_{1-x}F_xBiS_2$ by suppressing Ce^{3+}-Ce^{4+} valence fluctuation [39,40]. In the self-doped Eu systems, Eu^{2+}-Eu^{3+} mixed valence is consistent with the photoemission results [41]. While in the Ce system, the doped electrons are partially localized and are not consistent with the nominal x in $RO_{1-x}F_xBiS_2$. In this connection, the nature of valence states in $CeO_{1-x}F_xBiS_2$ ($x = 0$ to 0.5) are crucial and thus are quantitatively evaluated in Fig. 2. The Shirley-type background is removed from the Ce $3d$ peaks of $CeO_{1-x}F_xBiS_2$ ($x = 0, 0.5$) and nine Gaussian peaks are fit on the Ce $3d$. The Gaussian peaks are assigned for the $4f^2$, $4f^1$, and $4f^0$ contributions in Ce $3d_{5/2}$ and $3d_{3/2}$ from $CeO_{1-x}F_xBiS_2$ ($x = 0$, 0.5). The peaks are shifted by $\sim 0.10 \pm 0.05$ eV toward higher binding energy from $x = 0$ to 0.5 in $CeO_{1-x}F_xBiS_2$. It shows that the intensity of $4f^0$ is almost suppressed while going from $x = 0$ [Fig. 2(a)] to $x = 0.5$ [Fig. 2(b)]. This is consistent with the previous XAS work by Sugimoto *et al.* [30]. The Ce^{3+}/Ce^{4+} intensity ratio is evaluated from the relative intensity between $4f^1$ (Ce^{3+}) and $4f^0$ (Ce^{4+}) for Ce $3d_{5/2}$, indicated as peak 3 and 4 respectively in Fig. 2, and reveals an almost twofold (~1.89) decrease in Ce^{4+} from $x = 0$ to 0.5.

In Fig. 3(a), the Pr $3d$ spectra of $PrO_{1-x}F_xBiS_2$ ($x = 0.3$ and 0.5) show shifting of $\sim 0.10 \pm 0.05$ eV towards higher binding energy by the F doping (inset). The direction of Pr $3d$ shifting is consistent with electron doping. The spectral features of Pr $3d$ for $x = 0.3$ and 0.5 show features similar to those of the case of Pr_6O_{11}, where Pr^{3+} and Pr^{4+} coexist [42]. Pr $3d$ XPS from $PrO_{1-x}F_xBiS_2$ ($x = 0.3$, 0.5) shows a coexistence of Pr^{3+} and Pr^{4+} spectral features, as shown in Fig. 3(a) [35,42–44]. In Fig. 3(b), Pr $4d$ XPS has the shoulders around the main peak (~117 eV), showing little change apart from shifting toward higher binding energy with electron doping (inset). The interplay of intra-atomic multiplet coupling and solid-state hybridization can also be related with spectral features of $3d$ and $4d$, including the satellites [38]. However, the effect of the solid-state hybridization in Pr_6O_{11} and $PrO_{1-x}F_xBiS_2$ ($x = 0.3$ and 0.5) would be different. The solid-state hybridization is present between the $4f$ and O $2p$ with $4f^1\underline{L}$ and $4f^2\underline{L}^2$ charge-transfer satellites where ($\underline{L}$) represents a hole at the O $2p$ [36]. In Fig. 3(c), the Bi $4f$ spectra show a shift by $\sim 0.12 \pm 0.01$ eV toward the higher-binding-energy side from $x = 0.3$ to 0.5 for $PrO_{1-x}F_xBiS_2$ due to electron doping.

The possibility of the Pr^{3+}-Pr^{4+} mixed valence was recently examined for $x = 0.13$ and 0.23 in $PrO_{1-x}F_xBiS_2$, and the spectral features were a bit ambiguous due to lack of a detailed peak-fitting study [35]. Therefore, we used multiple peaks to fit the Pr $3d$ of $PrO_{1-x}F_xBiS_2$ ($x = 0.3$, 0.5) in Fig. 4. The Pr $3d$ of $PrO_{1-x}F_xBiS_2$ ($x = 0.3$, 0.5) are subtracted by the Shirley-type background and fit with six Gaussians ascribing $4f^3$, $4f^2$, and $4f^1$, as shown in Figs. 4(a) and 4(b), respectively. The peak at ~957 eV on the

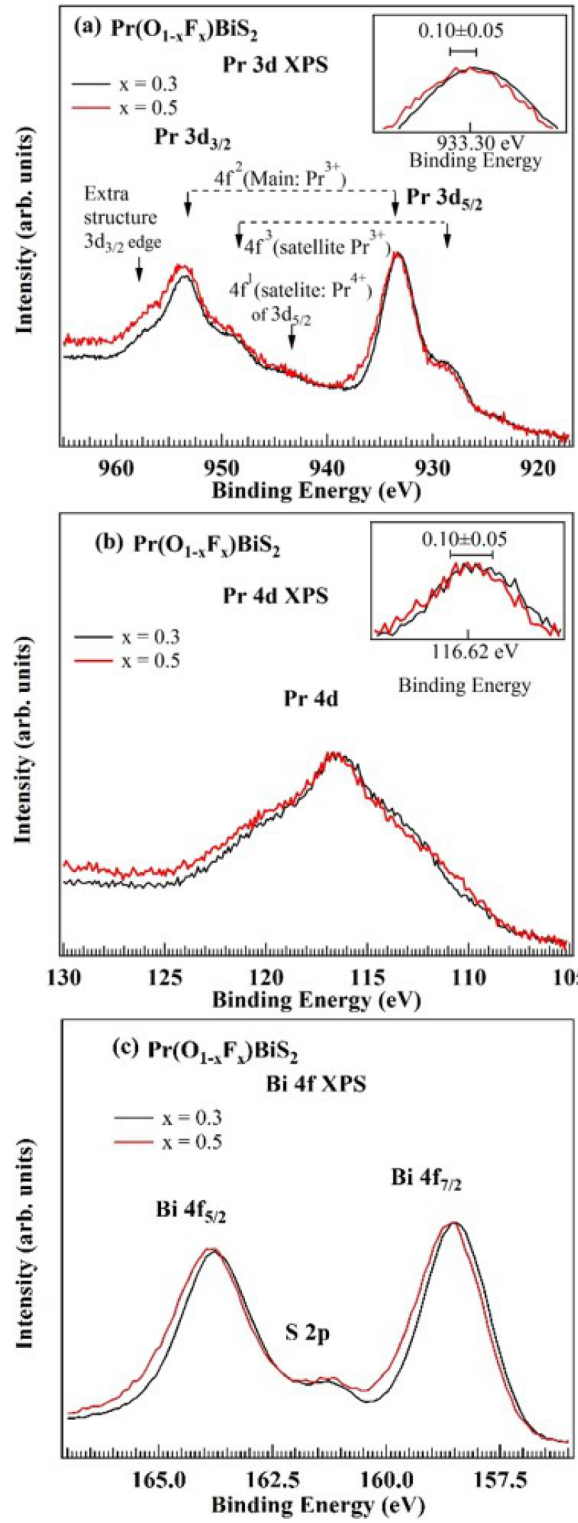

FIG. 3. XPS of (a) Pr $3d$, (b) Pr $4d$, and (c) Bi $4f$ from $PrO_{1-x}F_xBiS_2$ ($x = 0.3$, 0.5) at room temperature.

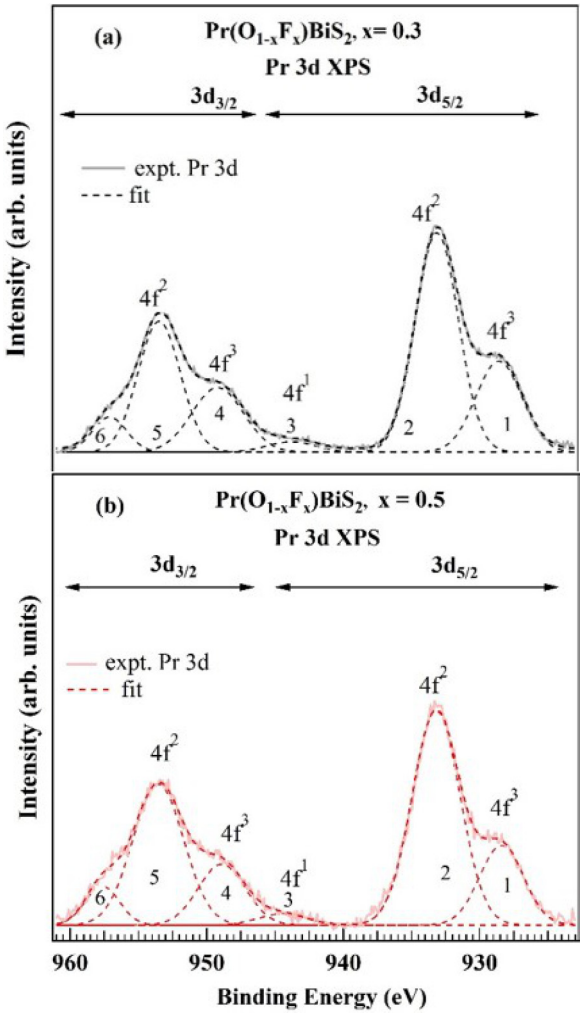

FIG. 4. XPS of Pr $3d$ with Gaussian fittings from $PrO_{1-x}F_xBiS_2$ for (a) $x = 0.3$ and (b) $x = 0.5$ at room temperature.

higher-binding-energy side of Pr $3d_{3/2}$ from $PrO_{1-x}F_xBiS_2$ ($x = 0.3$, 0.5) is ascribed as an extra structure of $3d_{3/2}$ [38]. Therefore, the Pr^{3+}/Pr^{4+} intensity ratio is estimated from the peak area of $4f^2$ (Pr^{3+}) and $4f^1$ (Pr^{4+}) of Pr $3d_{5/2}$ shown as peaks 2 and 3, respectively, in Fig. 4. It was found that Pr^{3+}/Pr^{4+} is almost constant with the electron doping from $x = 0.3$ to 0.5. This shows that the addition of the electrons from $x = 0.3$ to 0.5 do not involve the $4f^1$ (Pr^{4+}) and $4f^2$ (Pr^{3+}) components, but instead only shifts the binding energy of the core levels away from the Fermi level.

In addition to this, the Bi $4f_{7/2}$ peak shifts toward the higher-binding-energy side from $CeO_{0.5}F_{0.5}BiS_2$ to $PrO_{0.5}F_{0.5}BiS_2$ at room temperature, as shown in Fig. 5. The peak positions of Bi $4f_{7/2}$ obtained from Gaussians fit on Bi $4f$ from $PrO_{1-x}F_xBiS_2$ ($x = 0.3$, 0.5) and $CeO_{1-x}F_xBiS_2$ ($x = 0$, 0.5) at room temperature are summarized in Fig. 6 and shift away from the Fermi level with the F doping. In $LaO_{1-x}F_xBiS_2$ ($x = 0$ to 0.5) [45], the shift of Bi $4f_{7/2}$ is around 0.3 eV with electron doping, similar to the case of shifting of Bi $4f_{7/2}$ in Pr systems. While in the Ce systems, the Bi $4f_{7/2}$ shift is less compared with the Pr system (Fig. 6) and the Ce^{3+}-Ce^{4+} mixed valence is suppressed. The electron

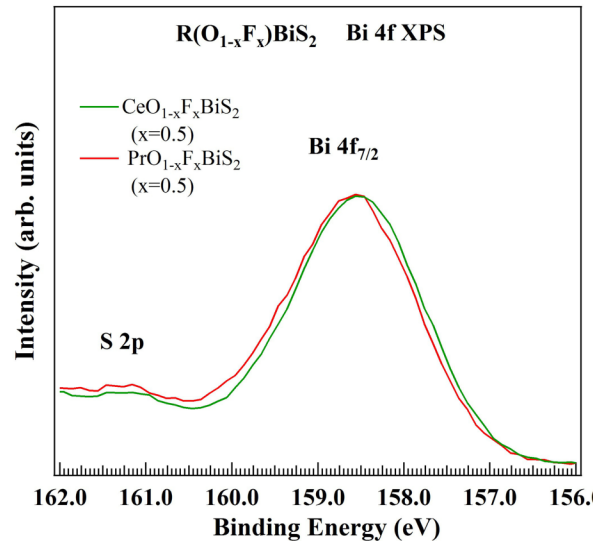

FIG. 5. XPS of Bi $4f$ from $PrO_{1-x}F_xBiS_2$ and $CeO_{1-x}F_xBiS_2$ for $x = 0.5$ at room temperature.

occupation of the $4f$ orbitals due to electron doping is different for the Ce and Pr systems. The shift in Ce $3d$ and Pr $3d$ with electron doping was calculated from the Gaussian fits, as shown in Figs. 2 and 4. The Ce^{3+}-Ce^{4+} valence fluctuations is suppressed while Pr^{3+}-Pr^{4+} mixed valence remains unchanged by F doping. In addition, the slope of the Bi $4f_{7/2}$ binding energy is larger in the Pr system than in the Ce system. While the Ce valence is almost +3 at $x = 0.5$ in the Ce system, the Pr^{3+}-Pr^{4+} mixed valence still remains at $x = 0.5$ in the Pr system. The electron occupation of the $6p$ hybridized orbitals due to doping could be different for the Ce and Pr systems.

IV. CONCLUSION

We have studied the electronic structure of $CeO_{1-x}F_xBiS_2$ ($x = 0$, 0.5) and $PrO_{1-x}F_xBiS_2$ ($x = 0.3$, 0.5) by means of XPS. The core-level photoemission spectra shift toward higher binding energy with F doping. In $CeO_{1-x}F_xBiS_2$

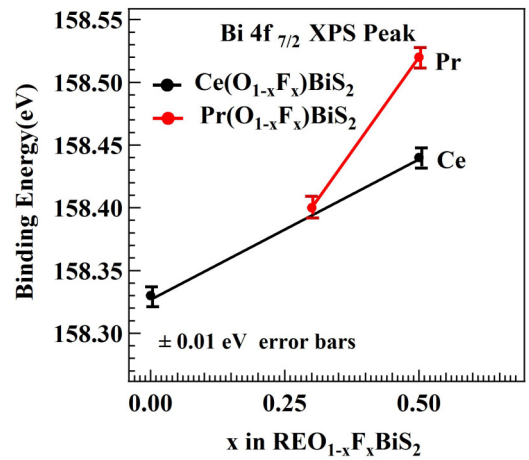

FIG. 6. Position of Bi $4f_{7/2}$ obtained from Gaussian fitting from $PrO_{1-x}F_xBiS_2$ ($x = 0.3$, 0.5) and $CeO_{1-x}F_xBiS_2$ ($x = 0$, 0.5) at room temperature.

($x = 0.5$), the doped electrons suppress the Ce^{4+} contribution and valence fluctuation, which is consistent with the early studies. The decrease in the valence fluctuation is associated with the decrease of Ce^{4+} components due to an increase of Bi $6p_z$ orbital occupations by electron doping. The suppression of valence fluctuations is related to the onset of superconductivity in $CeO_{1-x}F_xBiS_2$ from $x = 0$ to 0.5. In $PrO_{1-x}F_xBiS_2$ ($x = 0.3$, 0.5), the doped electrons do not suppress the Pr^{3+}-Pr^{4+} valence fluctuation. Rather, it increases the shifting of the Bi $4f_{7/2}$ away from the Fermi level higher and T_c is enhanced from $x = 0.3$ to 0.5. However, the Pr^{3+}-Pr^{4+} valence fluctuation still remains at $x = 0.5$ in the $PrO_{1-x}F_xBiS_2$. The difference in valence fluctuation between the Ce and Pr systems is associated with the difference in the magnetic properties.

ACKNOWLEDGMENTS

We would like to acknowledge Prof. Y. Mizuguchi and Prof. Y. Takano for the fruitful discussion, and Mr. T. Asano and T. Nakajima for the sample preparation. The present work was supported by CREST-JST (Grant No. JPMJCR15Q2) and MEXT/JSPS KAKENHI Grants No. 15H03693, No. 15H05884, No. 16J05692, and No. 16K05454.

[1] Y. Mizuguchi, H. Fujihisa, Y. Gotoh, K. Suzuki, H. Usui, K. Kuroki, S. Demura, Y. Takano, H. Izawa, and O. Miura, Phys. Rev. B **86**, 220510(R) (2012).
[2] S. K. Singh, A. Kumar, B. Gahtori, G. Sharma, S. Patnaik, and V. P. S. Awana, J. Am. Chem. Soc. **134**, 16504 (2012).
[3] Shruti, P. Srivastava, and S. Patnaik, J. Phys.: Condens. Matter **25**, 312202 (2013).
[4] G. Baskaran, Supercond. Sci. Technol. **29**, 124002 (2016).
[5] Y. Mizuguchi, S. Demura, K. Deguchi, Y. Takano, H. Fujihisa, Y. Gotoh, H. Izawa, and O. Miura, J. Phys. Soc. Jpn. **81**, 114725 (2012).
[6] V. P. S. Awana, A. Kumar, R. Jha, S. K. Singh, A. Pal Shruti, J. Saha, and S. Patnaik, Solid State Commun. **157**, 21 (2013).
[7] D. Yazici, K. Huang, B. D. White, A. H. Chang, A. J. Friedman, and M. B. Maple, Philos. Mag. **93**, 673 (2012).
[8] D. Yazici, K. Huang, B. D. White, I. Jeon, V. W. Burnett, A. J. Friedman, I. K. Lum, M. Nallaiyan, S. Spagna, and M. B. Maple, Phys. Rev. B **87**, 174512 (2013).
[9] R. Jha, A. Kumar, S. K. Singh, and V. P. S. Awana, J. Supercond. Novel Magn. **26**, 499 (2013).
[10] R. Jha, A. Kumar, S. K. Singh, and V. P. S. Awana, J. Appl. Phys. **113**, 056102 (2013).
[11] K. Deguchi, Y. Mizuguchi, S. Demura, H. Hara, T. Watanabe, S. J. Denholme, M. Fujioka, H. Okazaki, T. Ozaki, H. Takeya. Yamaguchi, O. Miura, and Y. Takano, Europhys. Lett. **101**, 17004 (2013).
[12] S. Demura, Y. Mizuguchi, K. Deguchi, H. Okazaki, H. Hara, T. Watanabe, S. J. Denholme, M. Fujioka, T. Ozaki, H. Fujihisa, Y. Gotoh, O. Miura, T. Yamaguchi, H. Takeya, and Y. Takano, J. Phys. Soc. Jpn. **82**, 033708 (2013).
[13] J. Xing, S. Li, X. Ding, H. Yang, and H.-H. Wen, Phys. Rev. B **86**, 214518 (2012).
[14] D. Yazici, I. Jeon, B. D. White, and M. B. Maple, Phys. C (Amsterdam, Neth.) **514**, 218 (2015).
[15] R. Jha, H. Kishan, and V. P. S. Awana, J. Appl. Phys. **115**, 013902 (2014).
[16] S. Demura, K. Deguchi, Y. Mizuguchi, K. Sato, R. Honjyo, A. Yamashita, T. Yamaki, H. Hara, T. Watanabe, S. J. Denholme, M. Fujioka, H. Okazaki, T. Ozaki, O. Miura, T. Yamaguchi, H. Takeya, and Y. Takano, J. Phys. Soc. Jpn. **84**, 024709 (2015).
[17] R. Higashinaka, T. Asano, T. Nakashima, K. Fushiya, Y. Mizuguchi, O. Miura, T. D. Matsuda, and Y. Aoki, J. Phys. Soc. Jpn. **84**, 023702 (2015).
[18] M. Nagao, A. Miura, S. Watauchi, Y. Takano, and I. Tanaka, Jpn. J. Appl. Phys. (1962–1981) **54**, 083101 (2015).
[19] M. Nagao, Novel Supercond. Mater. **1**, 64 (2015).
[20] Y. Mizuguchi, J. Phys. Chem. Solids **84**, 34 (2015).
[21] H. Usui, K. Suzuki, and K. Kuroki, Phys. Rev. B **86**, 220501(R) (2012).
[22] T. Sugimoto, D. Ootsuki, C. Morice, E. Artacho, S. S. Saxena, E. F. Schwier, M. Zheng, Y. Kojima, H. Iwasawa, K. Shimada, M. Arita, H. Namatame, M. Taniguchi, M. Takahashi, N. L. Saini, T. Asano, R. Higashinaka, T. D. Matsuda, Y. Aoki, and T. Mizokawa, Phys. Rev. B **92**, 041113(R) (2015).
[23] C. Morice, E. Artacho, S. E. Dutton, D. Molnar, H.-J. Kim, and S. S. Saxena, J. Phys.: Condens. Matter **28**, 345504 (2016).
[24] G. Lamura, T. Shiroka, P. Bonfà, S. Sanna, R. De Renzi, C. Baines, H. Luetkens, J. Kajitani, Y. Mizuguchi, O. Miura, K. Deguchi, S. Demura, Y. Takano, and M. Putti, Phys. Rev. B **88**, 180509(R) (2013).
[25] B. Li, Z. W. Xing, and G. Q. Huang, Europhys. Lett. **101**, 47002 (2013).
[26] X. Wan, H. C. Ding, S. Y. Savrasov, and C. G. Duan, Phys. Rev. B **87**, 115124 (2013).
[27] J. Lee, M. B. Stone, A. Huq, and T. Yildirium, Phys. Rev. B **87**, 205134 (2013).
[28] T. Yildirim, Phys. Rev. B **87**, 020506(R) (2013).
[29] Y. Wakisaka, K. Takubo, T. Sudayama, J.-Y. Son, T. Mizokawa, M. Arita, H. Namatame, M. Taniguchi, S. Sekiya, K. Fukuda, F. Ishikawa, and Y. Yamada, J. Phys. Soc. Jpn. **77**, 074710 (2008).
[30] T. Sugimoto, B. Joseph, E. Paris, A. Iadecola, T. Mizokawa, S. Demura, Y. Mizuguchi, Y. Takano, and N. L. Saini, Phys. Rev. B **89**, 201117(R) (2014).
[31] T. Agatsuma and T. Hotta, J. Magn. Magn. Mater. **400**, 73 (2016).
[32] L. K. Zeng, X. B. Wang, J. Ma, P. Richard, S. M. Nie, H. M. Weng, N. L. Wang, Z. Wang, T. Qian, and H. Ding, Phys. Rev. B **90**, 054512 (2014).
[33] Z. R. Ye, H. F. Yang, D. W. Shen, J. Jiang, X. H. Niu, D. L. Feng, Y. P. Du, X. G. Wan, J. Z. Liu, X. Y. Zhu, H. H. Wen, and M. H. Jiang, Phys. Rev. B **90**, 045116 (2014).
[34] T. Sugimoto, D. Ootsuki, E. Paris, A. Iadecola, M. Salome, E. F. Schwier, H. Iwasawa, K. Shimada, T. Asano, R. Higashinaka, T. D. Matsuda, Y. Aoki, N. L. Saini, and T. Mizokawa, Phys. Rev. B **94**, 081106(R) (2016).
[35] S. Ishii, Y. Hongu, A. Miura, and M. Nagao, Appl. Phys. Express **9**, 063101 (2016).
[36] S. Hüfner, *Photoelectron Spectroscopy* (Springer-Verlag, Berlin, Heidelberg, 2003).
[37] A. Fujimori, Phys. Rev. B **28**, 2281(R) (1983).

[38] H. Ogasawara, A. Kotani, R. Potze, G. A. Sawatzky, and B. T. Thole, Phys. Rev. B **44**, 5465 (1991).

[39] E. Paris, B. Joseph, A. Iadecola, T. Sugimoto, L. Olivi, S. Demura, Y. Mizuguchi, Y. Takano, T. Mizokawa, and N. L. Saini, J. Phys.: Condens. Matter **26**, 435701 (2014).

[40] M. Nagao, A. Miura, I. Ueta, S. Watauchi, and I. Tanaka, Solid State Commun. **245**, 11 (2016).

[41] E. Paris, T. Sugimoto, T. Wakita, A. Barinov, K. Terashima, V. Kandyba, O. Proux, J. Kajitani, R. Higashinaka, T. D. Matsuda, Y. Aoki, T. Yokoya, T. Mizokawa, and N. L. Saini, Phys. Rev. B **95**, 035152 (2017).

[42] A. A. Yaremchenko, S. G. Patrício, and J. R. Frade, J. Power Sources **245**, 557 (2014).

[43] M. Y. Sinev, G. W. Graham, L. P. Haack, and M. Shelef, J. Mater. Res. **11**, 1960 (1996).

[44] S. Lütkehoff, M. Neumann, and A. Ślebarski, Phys. Rev. B **52**, 13808 (1995).

[45] S. Nagira, J. Sonoyama, T. Wakita, M. Sunagawa, Y. Izumi, T. Muro, H. Kumigashira, M. Oshima, K. Deguchi, H. Okazaki, Y. Takano, O. Miura, Y. Mizuguchi, K. Suzuki, H. Usui, K. Kuroki, K. Okada, Y. Muraoka, and T. Yokoya, J. Phys. Soc. Jpn. **83**, 033703 (2014).